

Antineutrinos from Earth: A reference model and its uncertainties

Fabio Mantovani,^{1,2,3,*} Luigi Carmignani,^{1,2,†}

Gianni Fiorentini,^{4,3,‡} and Marcello Lissia^{5,6,§}

¹*Dipartimento di Scienze della Terra,*

Università di Siena, I-53100 Siena, Italy

²*Centro di GeoTecnologie CGT, I-52027 San Giovanni Valdarno, Italy*

³*Istituto Nazionale di Fisica Nucleare,*

Sezione di Ferrara, I-44100 Ferrara, Italy

⁴*Dipartimento di Fisica, Università di Ferrara, I-44100 Ferrara, Italy*

⁵*Istituto Nazionale di Fisica Nucleare,*

Sezione di Cagliari, I-09042 Monserrato (CA), Italy

⁶*Dipartimento di Fisica, Università di Cagliari, I-09042 Monserrato (CA), Italy*

(Dated: August 31, 2003; revised November 25, 2003)

Abstract

We predict geoneutrino fluxes in a reference model based on a detailed description of Earth's crust and mantle and using the best available information on the abundances of uranium, thorium, and potassium inside Earth's layers. We estimate the uncertainties of fluxes corresponding to the uncertainties of the element abundances. In addition to distance integrated fluxes, we also provide the differential fluxes as a function of distance from several sites of experimental interest. Event yields at several locations are estimated and their dependence on the neutrino oscillation parameters is discussed. At Kamioka we predict $N(U + Th) = 35 \pm 6$ events for 10^{32} proton yr and 100% efficiency assuming $\sin^2(2\theta) = 0.863$ and $\delta m^2 = 7.3 \times 10^{-5} \text{ eV}^2$. The maximal prediction is 55 events, obtained in a model with fully radiogenic production of the terrestrial heat flow.

PACS numbers: 91.35.-x, 13.15.+g, 14.60.Pq, 23.40.Bw

*Electronic address: mantovani@fe.infn.it

†Electronic address: luigi.carmignani@unisi.it

‡Electronic address: fiorenti@fe.infn.it

§Electronic address: marcello.lissia@ca.infn.it

I. INTRODUCTION

By looking at antineutrinos from reactors, KamLAND [1] has confirmed the oscillation phenomenon previously discovered by SNO [2] with solar neutrinos and has provided crucial information on the oscillation parameters. Putting together the results of solar and terrestrial experiments, the best fit is obtained at $\delta m^2 = 7.3 \times 10^{-5} \text{ eV}^2$ and $\sin^2(2\theta) = 0.863$ [3]. Since we know their fate from production to detection, neutrinos can now be used as physical probes.

Furthermore, the detector is so pure and the sensitivity is so high that KamLAND will be capable of studying geoneutrinos, the antineutrinos originating from Earth's natural radioactivity. Indeed, from a fit to the experimental data the KamLAND Collaboration reported four events associated with ^{238}U and five with ^{232}Th decay chains. This result, obtained from an exposure of just 162 ton yr, provides the first insight into the radiogenic component of the terrestrial heat. KamLAND has thus opened a new window for studying Earth's interior and one expects more precise results in the near future from KamLAND and other detectors which are presently in preparation.

The argument of geoneutrinos was introduced by Eder [4] in the 1960's and it was extensively reviewed by Krauss *et al.* [5] in the 1980's. Raghavan *et al.* [6] and Rothschild *et al.* [7]¹ remarked on the potential of KamLAND and Borexino for geoneutrino observations. Fiorentini *et al.* [8, 9, 10] discussed the relevance of geoneutrinos for determining the radiogenic contribution to Earth's heat flow and their potential for improving our knowledge of oscillation parameters, see also Ref. [11].

In preparation to the data which will become available in the near future, we present a systematic discussion of geoneutrinos, which incorporates the best geological and geochemical information on their sources and outlines the main uncertainties, so as to understand what can be gained from the study of geoneutrinos concerning both Earth's interior and neutrino properties. With this spirit, we shall consider the following points.

(i) We provide a reference model that incorporates the best available knowledge for the distribution of U, Th, and K in Earth's interior.

(ii) Within this model we predict neutrino fluxes and signals for detectors at different

¹ We shall always refer to the version available as arXiv:nucl-ex/9710001.

positions on Earth.

(iii) We estimate uncertainties of neutrino fluxes and signals corresponding to uncertainties of the U, Th, and K distributions.

II. THE REFERENCE MODEL: ELEMENT DISTRIBUTIONS AND GEONEUTRINO FLUXES

A global look at Earth's interior is useful before entering a detailed discussion on the element distributions. The amount of information which we (assume to) have on Earth's interior is somehow surprising, if one considers that the deepest hole which has ever been dug is probably only ten kilometers deep, a mere dent in planetary terms.

The outer layer is the relatively thin crust, divided in two types, continental crust (CC) and oceanic crust (OC). The former averages 38 km in thickness, varying around the globe from 20 to 70 km, and it is made primarily of light elements such as potassium, sodium, silicon, calcium, and aluminium silicates. The oceanic crust is much thinner, from about 6 to 8 km.

Inside this crustal skin is Earth's mantle which is 2900 km deep overall. Largely made up of iron and magnesium silicates, the mantle as a whole accounts for about 68% of Earth's mass. One distinguishes the upper mantle ² (UM) from the lower mantle (LM), however, the seismic discontinuities between the two parts do not necessarily divide the mantle into layers. The main questions about the mantle are does it move as a single layer or as multiple layers? Is it homogeneous in composition or heterogeneous? How does it convect? These questions sound simple, but the answers are complex, possibly leading to more questions, see Ref. [12].

Inside the mantle is Earth's core, which accounts for about 32% of Earth's mass. Based on comparison with the behavior of iron at high pressures and temperatures in laboratory experiments, on the seismic properties of the core, and on the fact that iron is the only sufficiently abundant heavy element in the universe, the core is generally believed to be made primarily of iron with small amounts of nickel and other elements. Over thirty years ago, however, it was suggested that a significant amount of potassium could be hidden in

² We shall define the upper mantle as the shallow mantle plus the transition region, i.e., the region below the crust down to 677 km [15].

Earth’s core, thus providing a large fraction of the terrestrial heat flow through ^{40}K decay. This controversial possibility has been revived recently in Ref. [13].

Uranium, thorium, and potassium are lithophile elements, which accumulate in the continental crust. Their abundance in the mantle is much smaller, however, the total amounts are comparable with those in the crust, due to the much larger mantle mass. The core is generally believed to contain negligible amounts of these elements.

A global description of the present crust-plus-mantle system is provided by the bulk silicate earth (BSE) model, a reconstruction of the primordial mantle of Earth, subsequent to the core separation and prior to crust differentiation, based on geochemical arguments. In the BSE model the uranium abundance ³ is $a_{\text{BSE}}(\text{U}) = 2 \times 10^{-8}$, and one has $\text{Th}/\text{U} \equiv a(\text{Th})/a(\text{U}) = 3.9$ and $\text{K}/\text{U} \equiv a(\text{K})/a(\text{U}) = 1.14 \times 10^4$, where the quoted values are averages between different estimates, all consistent with each other to the level of 10% or better, see Table I. In the BSE model the total masses of uranium, thorium and potassium are thus $M(\text{U}) = 0.81 \times 10^{17}$ kg, $M(\text{Th}) = 3.16 \times 10^{17}$ kg, and $M(\text{K}) = 0.49 \times 10^{21}$ kg.

The equation relating masses and heat production is

$$H = 9.5M(\text{U}) + 2.7M(\text{Th}) + 3.6M(\text{K}) \quad , \quad (1)$$

where H is in TW, $M(\text{U})$ and $M(\text{Th})$ are in units of 10^{17} kg, and $M(\text{K})$ in units of 10^{21} kg.

In the BSE model, the contributed heat production rates are $H(\text{U}) = 7.6$ TW, $H(\text{Th}) = 8.5$ TW, and $H(\text{K}) = 1.8$ TW, for a total of about one half of the observed terrestrial heat flow ($H_E \approx 40$ TW).

A. Uranium, thorium, and potassium distributions

Our aim is to build a reference model (labeled as “ref”), which incorporates the best available knowledge of U, Th and K distributions inside Earth. Concerning Earth’s crust, we distinguish oceans and seawater, the continental crust, subdivided into three sublayers (upper, middle, and lower), sediments and oceanic crust. All these layers have been mapped in Ref. [14], which provides values of density and depth over the globe on a grid with 2° steps. We distinguish next the upper mantle (extending down to about 600 km), the lower mantle

³ We shall always refer to element abundances in mass and we remind the reader that the natural isotopic composition is $^{238}\text{U}/\text{U} = 0.993$, $^{232}\text{Th}/\text{Th} = 1$ and $^{40}\text{K}/\text{K} = 1.2 \times 10^{-4}$.

(down to about 2900 km), and the core, and use the preliminary reference earth model (PREM) [15] for the values of the density at each depth, assuming spherical symmetry.

For each component, one has to adopt a value for the abundances $a(\text{U})$, $a(\text{Th})$, and $a(\text{K})$. In the literature of the last twenty years one can find many estimates of abundances for the various components of the crust (OC, upper CC, lower CC, ...), generally without an error value (see Tables II, III, and IV), two classical reviews being in Refs. [16, 17] and a most useful source being provided by the GERM Reservoir database [18].

For the upper mantle we are aware of several estimates by Jochum *et al.* [19], White [20], O’Nions and McKenzie [21], Hofmann [22], and Zartman and Haines [23]. In this respect data obtained from material emerged from unknown depths are assumed to be representative of the average composition down to about 600 km.

For each (sub)layer of the crust and for the upper mantle, we adopt as reference value for the uranium abundance $a^{\text{ref}}(\text{U})$ the average of the values reported in Tables II, III, and IV. Concerning Th and K, we observe that the abundance ratios with respect to uranium are much more consistent among different authors than the corresponding absolute abundances. We shall thus take the average of ratios and from these construct the reference abundances for thorium and potassium:

$$a^{\text{ref}}(\text{Th}) = \langle \text{Th/U} \rangle a^{\text{ref}}(\text{U}) \quad \text{and} \quad a^{\text{ref}}(\text{K}) = \langle \text{K/U} \rangle a^{\text{ref}}(\text{U}) \quad . \quad (2)$$

For the lower mantle, where no observational data are available, we resort to the BSE model, which — we recall — describes the present crust-plus-mantle system based on geochemical arguments.

The mass of each element ($X = \text{U}, \text{Th}, \text{K}$) in the lower mantle $M_{\text{LM}}(X)$ is thus obtained by subtracting from the BSE estimate the mass calculated for the crust and upper mantle:

$$M_{\text{LM}}(X) = M_{\text{BSE}}(X) - M_{\text{CC}}(X) - M_{\text{OC}}(X) - M_{\text{UM}}(X) \quad . \quad (3)$$

Reference abundances for the lower mantle are then obtained by dividing these values by its mass $M_{\text{LM}} = 2.9 \times 10^{24}$ kg. According to geochemical arguments, negligible amounts of U, Th and K should be present in the core.

The resulting choice of input values for the reference model is collected in Tables II, III, and IV. Concerning this reference model, we remark the following points.

- (i) The uranium mass in the crust $M_{\text{c}}(\text{U}) = 0.35 \times 10^{17}$ kg is mainly concentrated in

the continental part. The oceanic crust contributes as little as 0.005×10^{17} kg, since its impoverished by a factor of 20 and it is much thinner than the continental crust.

(ii) The estimated uranium mass in the upper mantle is about one sixth of that in the crust, whereas the lower mantle contains about as much uranium as the crust.

(iii) Note that in this reference model, constructed so as to satisfy the BSE constraint (3), mantle depletion (with respect to BSE) extends to the lower mantle.

(iv) Similar considerations hold for thorium and potassium.

B. The reference fluxes

For each element X the produced ⁴ antineutrino fluxes at position \vec{r} are defined as

$$\Phi_X(\vec{r}) = \frac{n_X}{4\pi\mu_X\tau_X} \int_{V_\oplus} d\vec{r}' \frac{\rho(\vec{r}')a_X(\vec{r}')}{|\vec{r} - \vec{r}'|^2} , \quad (4)$$

where τ is the lifetime, μ is the atom mass, n is the number of antineutrinos per decay chain, the integral is over the volume of the earth, ρ is the local density, and a_X is the abundance of the element X . We have evaluated the produced fluxes at several sites on the globe within the reference model ($a = a^{\text{ref}}$). We concentrate here on a few locations of specific interest, see Tables V, VI, and VII.

(i) for the Kamioka mine, where the KamLAND detector is in operation, we predict an uranium flux $\Phi_U = 3.7 \times 10^6 \text{ cm}^{-2} \text{ s}^{-1}$, a comparable flux from thorium and a fourfold flux from potassium. Within the reference model, about 3/4 of the flux is generated from material in the crust and the rest mainly from the lower mantle.

(ii) At Gran Sasso laboratory, where Borexino [24] is in preparation, we predict an uranium flux $\Phi_U = 4.2 \times 10^6 \text{ cm}^{-2} \text{ s}^{-1}$, this larger flux arising from a bigger contribution of the surrounding continental crust. Thorium and potassium fluxes are correspondingly rescaled.

(iii) At the top of Himalaya, a place chosen so that the crust contribution is maximal, we find the maximum uranium flux $\Phi_U = 6.7 \times 10^6 \text{ cm}^{-2} \text{ s}^{-1}$. The crust contribution exceeds 90%.

(iv) On the Hawaii, a site which minimizes the crust contribution, we find $\Phi_U = 1.3 \times 10^6 \text{ cm}^{-2} \text{ s}^{-1}$, originated mainly from the mantle.

⁴ The produced fluxes are calculated ignoring oscillations, which will be discussed later.

These computed reference fluxes are generally larger than those of Rothschild [7], by a factor of order 30–50 %. This arises from several differences in the approaches.

(i) We have used a more recent and detailed map of Earth’s crust: the grid is denser and several layers are distinguished.

(ii) We have a more detailed model for the mantle, corresponding to the PREM density profile.

(iii) Most important, our reference values for the abundances in the continental crust are larger than that used in Ref. [7]. As an example, Rothschild *et al.* use for the continental crust $a_{CC}(U) = 0.91$ ppm from a classical review paper of 1985 [16]. Our reference model, when averaged over the different sublayers, yields $a_{CC}(U) = 1.5$ ppm. This larger value arises from taking into account recent data, which are all higher than those quoted in Ref. [16].

The produced fluxes are computed ignoring the effect of oscillations, which depends on the distance R between the detector and the source. For taking into account this effect, and also in view of understanding which portion of Earth can be accessed with a geoneutrino detector, it is useful to introduce quantities which contain more detailed information.

The differential fluxes $f(R)$ are obtained by grouping together all the sources which lie at the same distance R from the detector

$$f_X(R) = \frac{n_X}{4\pi\mu_X\tau_X} \int_{V_\oplus} d\vec{r}' \frac{\rho(\vec{r}')a_X(\vec{r}')}{|\vec{r} - \vec{r}'|^2} \delta(R - |\vec{r} - \vec{r}'|) \quad . \quad (5)$$

Note that $f_X(R)$ actually depends also on the detector position \vec{r} and just for simplicity of notation we drop this variable.

The cumulated fluxes $\phi(R)$ are defined as

$$\phi_X(R) = \int_0^R dR' f_X(R') \quad . \quad (6)$$

They represent the cumulative effect of all sources within a distance R from the detector: the total produced fluxes of Eq. (4) are clearly $\Phi_X = \phi_X(2R_\oplus)$.

These quantities are plotted in Figs. 1 and 2 for the four sites (we only show the uranium contribution, the shapes of the other contributions being similar). We remark that we have been using an average density approximation, which presumably breaks down near the detector, where one should resort to a detailed geological study of the surroundings. From Fig. 2 one sees that in our model the region within 30 km from Kamioka or Gran Sasso originates about 15% of the total produced flux. Concerning the region where most of the

flux is generated, one sees again from Fig. 2 that 50% of the produced flux originated within 400 km (800 km) from Kamioka (Gran Sasso).

In Tables VIII, IX and X we present the numerical values of the contribution to $f_X(R)$ from the crust at Kamioka and Gran Sasso and that from the mantle (the assumed spherical symmetry of the mantle implies the same contribution at any site). These data will be useful for a detailed analysis of future experiments devoted to the study of geoneutrinos, in order to take into account the distance dependence of the survival probability.

III. THE UNCERTAINTIES OF THE REFERENCE MODEL

The fluxes of the reference model correspond to the best available knowledge about the crust and the interior of Earth, as derived from observational data and geochemical information on the global properties. An estimate of the uncertainties of the predicted fluxes is clearly useful.

Since the abundance ratios look relatively well determined, we concentrate on the uncertainties of the uranium abundances in the different layers and propagate them to the other elements. For the reference model, we have $M_{CC}(U) = 0.345 \times 10^{17}$ kg, $M_{OC}(U) = 0.005 \times 10^{17}$ kg, the total mass of CC being $M_{CC} = 2.234 \times 10^{22}$ kg. According to our model, the average uranium abundance in the CC is thus $a_{CC}(U) = 1.54 \times 10^{-6}$. We determine lower and upper limits by observing that the range of estimated uranium abundances is between 0.91×10^{-6} [16] and 1.8×10^{-6} [25]

$$\begin{aligned} \text{low: } & a_{CC}(U) = 0.9 \times 10^{-6}; a_{CC}(\text{Th}) = 3.7 \times 10^{-6}; a_{CC}(\text{K}) = 0.94 \times 10^{-2} \quad , \\ \text{high: } & a_{CC}(U) = 1.8 \times 10^{-6}; a_{CC}(\text{Th}) = 7.6 \times 10^{-6}; a_{CC}(\text{K}) = 1.97 \times 10^{-2} \quad . \end{aligned}$$

We remark that there is an overall uncertainty of a factor 2 concerning the total amount of radioactive materials in the crust.

For the upper mantle, we take as extrema the two values known to us [19, 23] for uranium and we deduce thorium and potassium by rescaling

$$\begin{aligned} \text{low: } & a_{UM}(U) = 5 \times 10^{-9}; a_{UM}(\text{Th}) = 13 \times 10^{-9}; a_{UM}(\text{K}) = 6 \times 10^{-5} \quad , \\ \text{high: } & a_{UM}(U) = 8 \times 10^{-9}; a_{UM}(\text{Th}) = 21 \times 10^{-9}; a_{UM}(\text{K}) = 9.6 \times 10^{-5} \quad . \end{aligned}$$

Such a small uncertainty is perhaps optimistic, however, it is not influential for the future discussion in view of the relatively small amounts contained in the upper mantle.

We remind the reader that no observational information is available for the lower mantle. For building a minimal model, we assume that the mantle is fully mixed and use for the whole mantle the lowest values estimated from samples coming from the upper mantle.

A maximal model can be obtained by assuming that the terrestrial heat is fully accounted by radiogenic production. This can be obtained by keeping the BSE abundance ratios fixed and rescaling the total masses to $M(\text{U}) = 1.67 \times 10^{17}$ kg, $M(\text{Th}) = 6.5 \times 10^{17}$ kg, and $M(\text{K}) = 1.9 \times 10^{21}$ kg.⁵ A natural implementation is obtained by choosing for the crust and upper mantle the highest observational estimates and placing the remaining mass in the lower mantle.

All this leads to

$$\begin{aligned} \text{low: } a_{LM}(\text{U}) &= 5 \times 10^{-9}; & a_{LM}(\text{Th}) &= 13 \times 10^{-9}; & a_{LM}(\text{K}) &= 6 \times 10^{-5} \quad , \\ \text{high: } a_{LM}(\text{U}) &= 40 \times 10^{-9}; & a_{LM}(\text{Th}) &= 156 \times 10^{-9}; & a_{LM}(\text{K}) &= 45.6 \times 10^{-5} \quad . \end{aligned}$$

The corresponding low and high estimates of the produced fluxes are also shown in Tables V, VI, and VII for a few locations.

In view of assigning an uncertainty to the fluxes of the reference model one can take two different approaches.

(a) A conservative estimate: the error assigned to the reference value is half of the difference between the high and low estimates $\Delta\Phi_{\text{cons}} = (\Phi_{\text{high}} - \Phi_{\text{low}})/2$.

(b) A statistical estimate: one assumes that the full range of calculated fluxes represents a $\pm 3\sigma$ interval.⁶ In this way one obtain a conventional 1σ error $\Delta\Phi = (\Phi_{\text{high}} - \Phi_{\text{low}})/6$.

The relative uncertainties of the fluxes are reported in Table XI. They are the same (and fully correlated) for all elements, the $1\text{-}\sigma$ error being about 15%, at Kamioka and Gran Sasso. At Hawaii, where the mantle contribution is dominant, the error is much larger, as a consequence of the large uncertainties of the lower mantle's composition.

When using these errors, one has to remark that uncertainties associated with abundances in the crust and in the upper mantle are deduced from the spread of observational data, whereas the estimates for the lower mantle, which cannot be accessed by observations, completely rely on theoretical arguments. In addition, one should also take into account the detailed geological structure around the detector for more precise flux estimates.

⁵ Clearly this model does not satisfy the BSE constraint on the total U, Th, and K masses in the Earth.

⁶ If unhappy with this conventional assumption, the reader can rescale σ .

IV. FROM FLUXES TO SIGNALS AND DETECTORS

Geoneutrinos can be detected by means of inverse beta reactions

$$\bar{\nu}_e + (Z, A) \rightarrow e^+ + (Z - 1, A) \quad , \quad (7)$$

where the positron kinetic energy T is related to the antineutrino energy E by $T = E - E_0$, with $E_0 = m_{Z-1} + m_e - m_Z$.⁷ The differential event yield as a function of T is given by

$$\frac{dN}{dT} = N_Z t \sigma(E) \sum_X w_X(E) \int_0^{2R_\oplus} dR f_X(R) P_{ee}(E, R) \quad , \quad (8)$$

where $N_Z t$ is the exposure (number of target nuclei times the live time), $\sigma(E)$ is the cross section of reaction (7), $T = E - E_0$ and the integral is over the distance R from the detector.

The survival probability of $\bar{\nu}_e$ produced at distance R with energy E is

$$P_{ee}(E, R) = 1 - \sin^2(2\theta) \sin^2\left(\frac{\delta m^2 R}{4E}\right) \quad . \quad (9)$$

For each element, the differential produced flux $f_X(R)$ is defined in Eq. (5), $w_X(E)$ is the energy spectrum of the $\bar{\nu}_e$ from the decay chain [26] of element X and normalized to 1, $\int_0^\infty dE w_X(E) = 1$. For simplicity we neglect the finite energy resolution of the detector and assume 100% detection efficiency.

Another interesting observable is the total geoneutrino yield

$$N = \int_0^{T_{\max}} dT \frac{dN}{dT} \quad , \quad (10)$$

where T_{\max} is the maximal positron energy.

The classical approach to low energy antineutrino detection is by using hydrogen compounds as target, by means of $\bar{\nu}_e + p \rightarrow e^+ + n$. Since $E_0 = m_n + m_e - m_p = 1.804$ MeV, this reaction is suitable for antineutrinos from uranium and thorium progenies ($E_{\max} = 3.26$ and 2.25 MeV, respectively), whereas antineutrinos from potassium ($E_{\max} = 1.31$ MeV) are below threshold.

⁷ A frequently used variable is the visible energy $E_{\text{vis}} = T + 2m_e$ which is the energy released in the slowing down and subsequent annihilation of the positron.

A. Total yields

We discuss first the total geoneutrino yield N , which is experimentally more accessible than the differential spectrum. In view of the structure of the survival probability, see Eq. (9), it can be written as

$$N = N_{\text{no}} [1 - \sin^2(2\theta)\chi(\delta m^2)] \quad , \quad (11)$$

where N_{no} is the yield for no oscillation.

The function χ depends on the uranium and thorium distributions inside Earth and on the detector position. Obviously χ tends to 0 (1/2) for small (large) values of δm^2 . We have computed χ in the reference model for some sites of interest, see Fig. 3. At all locations and for $\delta m^2 > 4 \times 10^{-5} \text{ eV}^2$, the function χ differs from its asymptotic value by less than 2%. Using the asymptotic value of the survival probability and the best fit value of the mixing angle [3], one finds

$$N = N_{\text{no}} [1 - 0.5 \sin^2(2\theta)] = 0.57 N_{\text{no}} \quad . \quad (12)$$

In Fig. 4 we show the relative contributions of different distances to the total yield: for the most interesting values of δm^2 the region within 30 km from Kamioka contributes about 15% of the total. The no oscillation yield N_{no} is determined in terms of the total produced fluxes from uranium and thorium [9]

$$N_{\text{no}} = 13.2\Phi_{\text{U}} + 4.0\Phi_{\text{Th}} \quad (13)$$

for an exposure of 10^{32} proton yr with fluxes Φ in units of $10^6 \text{ cm}^{-2} \text{ s}^{-1}$.

The no oscillation yields, calculated with the fluxes of the reference model, are shown in Table XII. In the same table we also present the estimated 1σ errors, obtained by propagating those on the produced fluxes (which are dominant over the other uncertainties from cross sections, decay spectrum, etc.) and the minimal and maximal predictions.

For the Kamioka site the prediction of the reference model (normalized ⁸ to 10^{32} proton yr and 100% efficiency) is $N_{\text{no}} = 61$ in good agreement with the ‘‘best model’’ of Refs. [8, 10], $N_{\text{no}} = 67$ TNU, in between the values of Ref. [7], $N_{\text{no}} = 43$ TNU, and of model 1b of

⁸ It is useful to introduce a terrestrial neutrino unit (TNU) for event rates, defined as one event per 10^{32} target nuclei per year, or $3.17110^{-40} \text{ s}^{-1}$ per target nucleus. This unit is analogous to the solar neutrino unit (SNU) [27].

Ref. [6], $N_{\text{no}} = 75$ TNU. An experimental value for $N_{\text{no}} = 156$ TNU can be deduced from the nine geoneutrinos reported by KamLAND, assuming $P_{ee} = 0.57$. All the above predictions are consistent with the experimental result within its statistical error (about 60% [9]).

The total yields predicted in our reference model for a number of locations are presented in Fig. 5. We remind the reader that geoneutrino fluxes are superimposed to the low-energy tail of antineutrinos from nuclear reactors, which can provide in this respect an important background, as first pointed out by Lagage [28]. This effect is clearly dependent on location and it has been extensively discussed in Ref. [10]. In particular, the event yield from reactors has been estimated as about 300 TNU (no oscillations) at Kamioka and about 70 TNU at Gran Sasso.

B. Event spectra

A more detailed information is contained in the event spectrum dN/dT and a relevant question is whether the spectrum is deformed because of oscillations. From Eqs (8) and (9) the event distribution with energy can be written as

$$\frac{dN}{dT} = \left(\frac{dN}{dT} \right)_{\text{no}} [1 - \sin^2(2\theta)\psi(T, \delta m^2)] \quad , \quad (14)$$

where T is the positron kinetic energy.

The no-oscillation spectrum dN_{no}/dT is shown in Fig. 6 for Kamikande. The function $\psi(T, \delta m^2)$ represents the modification to the event spectrum due to oscillations. It is plotted for Kamioka for a few values of δm^2 in Fig. 7. One sees that oscillations produce a moderate distortion for the two smallest values of δm^2 and the distortion is negligible for the largest values of δm^2 .

V. CONCLUDING REMARKS

We summarize here the main points of this paper

(i) We have provided a reference model for the produced fluxes of geoneutrinos, estimating its uncertainties in view of available data and geochemical inferences about U, Th, and K distribution in Earth's interior. When normalized to an exposure of 10^{32} proton yr, an averaged survival probability $\langle P_{ee} \rangle = 0.57$ and a 100% detection efficiency, the predicted

events for KamLAND are

$$N(\text{U}) = 28 \pm 4.7 \quad , \quad N(\text{Th}) = 7 \pm 1.2 \quad . \quad (15)$$

Errors have been estimated so as correspond to 1σ confidence level and are (almost) completely correlated:

$$N(\text{U} + \text{Th}) = 35 \pm 6 \quad . \quad (16)$$

(ii) Concerning the estimated errors, we remark that uncertainties associated with abundances in the crust and in the upper mantle are deduced from the spread of observational data, whereas the estimates for the lower mantle, which cannot be accessed by observations, completely rely on theoretical arguments. In addition, one should also take into account the detailed geological structure around the detector for more precise flux estimates.

(iii) We have also investigated extreme models, corresponding to the minimal and maximal amounts of U and Th which could be present on Earth. At KamLAND we predict

$$N^{\text{low}}(\text{U} + \text{Th}) = 29 \quad \text{and} \quad N^{\text{high}}(\text{U} + \text{Th}) = 74 \quad . \quad (17)$$

In these two extreme models U, Th, and K, in the BSE proportions, produce a radiogenic heat $H_{\text{rad}} = 9$ and 40 TW, respectively. If experimental results come out close to the minimum, then uranium and thorium provide a minor contribution to Earth's energetics: either Earth's heat flow is mainly non radiogenic or a significant amount of potassium has to be hidden in Earth's interior. If values near to the maximal are found from experiments, then radiogenic contribution is the main supply of Earth's heat flow, and one can exclude models where significant amounts of potassium are hidden in Earth's core.

(iv) Predictions for detectors at several locations are also given, see Table XII and Fig. 5. We remark that a detector located far from the continental crust could provide significant information on the structure of the mantle, particularly when compared with data from detectors at sites where (as in KamLAND and Borexino) the contribution of Earth's crust is important.

Acknowledgments

We are grateful for useful comments and discussions to B. Ricci, L. Beccaluva, T. Lasserre, E. Lisi, R. Marcolongo, G. Ottonello, S. Schönert, and R. Vannucci. This work was partially

supported by MIUR (Ministero dell'Istruzione, dell'Università e della Ricerca) under PRIN 2001 and PRIN 2002.

- [1] KamLAND Collaboration, K. Eguchi *et al.*, Phys. Rev. Lett. **90**, 021802 (2003) [arXiv:hep-ex/0212021].
- [2] SNO Collaboration, Q. R. Ahmad *et al.*, Phys. Rev. Lett. **89**, 011301 (2002) [arXiv:nucl-ex/0204008].
- [3] G. L. Fogli, E. Lisi, A. Marrone, D. Montanino, A. Palazzo, and A. M. Rotunno, Phys. Rev. D **67**, 073002 (2003) [arXiv:hep-ph/0212127].
- [4] G. Eder, Nucl. Phys. **78**, 657 (1966).
- [5] L. M. Krauss, S. L. Glashow, and D. N. Schramm, Nature (London) **310**, 191 (1984).
- [6] R. S. Raghavan, S. Schönert, S. Enomoto, J. Shirai, F. Suekane, and A. Suzuki, Phys. Rev. Lett. **80**, 635 (1998).
- [7] C. G. Rothschild, M. C. Chen, and F. P. Calaprice, Geophys. Res. Lett. **25**, 1083 (1998) [arXiv:nucl-ex/9710001].
- [8] G. Fiorentini, F. Mantovani, and B. Ricci, Phys. Lett. B **557**, 139 (2003) [arXiv:nucl-ex/0212008].
- [9] G. Fiorentini, T. Lasserre, M. Lissia, B. Ricci, and S. Schönert, Phys. Lett. B **558**, 15 (2003) [arXiv:hep-ph/0301042].
- [10] G. Fiorentini, M. Lissia, F. Mantovani, and B. Ricci, arXiv:physics/0305075.
- [11] H. Nunokawa, W. J. Teves, and R. Z. Funchal, arXiv:hep-ph/0308175.
- [12] *Chemical Reservoirs and Convection in the Earth's Mantle. Papers of a Discussion Meeting held at The Royal Society on 16 and 17 January, 2002*, edited by J. H. Davies, J. P. Brodholt and B. J. Wood (The Royal Society, London, 2002).
- [13] V. Rama Murthy, Win Van Westrenen, and Yingwei Fei, Nature (London) **423**, 163 (2003).
- [14] C. Bassin, G. Laske, and G. Masters, EOS Trans. Am. Geophys. Union **81**, F897 (2000) [<http://mahi.ucsd.edu/Gabi/rem.html>].
- [15] A. M. Dziewonski and D. L. Anderson, Phys. Earth Planet. Interact. **25**, 297 (1981).
- [16] S. R. Taylor and S. M. McLennan, *The Continental Crust: its Composition and Evolution* (Blackwell Scientific, Oxford, 1985).

- [17] K. H. Wedepohl, *Geochim. Cosmochim. Acta* **59**, 1217 (1995).
- [18] GERM, the Geochemical Earth Reference Model, is available on the web at <http://earthref.org>.
- [19] K. P. Jochum *et al.*, *Nature (London)* **322**, 221 (1986).
- [20] W. M. White, *Earth Planet Sci. Lett.* **115**, 211 (1993) [arXiv:hep-ph/0212202].
- [21] R. K. O’Nions, D. McKenzie, *Philos. Trans. R. Soc. London* **A342**, 65 (1993).
- [22] A. W. Hofmann, *Earth Planet Sci. Lett.* **90**, 297 (1988).
- [23] R. E. Zartman and S. Haines, *Geochim. Cosmochim. Acta* **52**, 1327 (1988).
- [24] BOREXINO Collaboration, G. Alimonti *et al.*, *Astropart. Phys.* **16**, 205 (2002).
- [25] D. M. Shaw, J. J. Cramer, M. D. Higgins, and M. G. Truscott, in *The Nature of the Lower Continental Crust*, edited by J. Dawson *et al.* (Geological Society of London, London, 1986), p. 275.
- [26] H. Behrens and J. Janecke, *Numerical Tables for Beta Decay and Electron Capture* (Springer-Verlag, Berlin, 1969).
- [27] J. N. Bahcall, *Neutrino Astrophysics* (Cambridge University Press., Cambridge, 1989), p. 3.
- [28] P. O. Lagage, *Nature (London)* **316**, 420 (1985).
- [29] W. F. McDonough, S. S. Sun, A. E. Ringwood, E. Jagoutz, and A. W. Hofmann, *Geochim. Cosmochim. Acta* **56**, 1001 (1992).
- [30] H. Wänke, G. Dreibus, and E. Jagoutz, in *Archean Geochemistry*, edited by A. Kroener, G N. Hanson, and A. M. Goodwin (Springer-Verlag, New York, 1984), pp. 1–24.
- [31] M. S. Quinby-Hunt and K. K. Turekian, *EOS Trans. Am. Geophys. Union* **64**, 130 (1983).
- [32] T. Plank and C. H. Langmuir, *Chem. Geol.* **145**, 325 (1998).
- [33] K. C. Condie, *Chem. Geol.* **104**, 1 (1993).
- [34] R. L. Rudnick and D. M. Fountain, *Rev. Geophys.* **33**, 267 (1995).

TABLE I: Abundances in the bulk silicate Earth model.

$a(\text{U})$	Th/U	K/U	Remarks
2.1×10^{-8}	4.0	1.14×10^4	[29]
2.3×10^{-8}			[30]
2.0×10^{-8}	4.0	1.27×10^4	[22]
1.8×10^{-8}	3.6	1.0×10^4	[16]
2.0×10^{-8}	3.9	1.14×10^4	average

TABLE II: Uranium abundances in Earth's interior.

Layer	Available data	Adopted value	Remarks
	$a(\text{U})$	$a^{\text{ref}}(\text{U})$	
Oceans & Seawater	3.2×10^{-9}	3.2×10^{-9}	[31]
Sediments	1.68×10^{-6}	1.68×10^{-6}	[32]
Upper CC	$(2.2 ; 2.4 ; 2.5 ; 2.8) \times 10^{-6}$	2.5×10^{-6}	Average of [33], [33], [17], [16]
Middle CC	1.6×10^{-6}	1.6×10^{-6}	[34]
Lower CC	$(0.20 ; 0.28 ; 0.93 ; 1.1) \times 10^{-6}$	0.62×10^{-6}	Average of [34], [16], [17], [25]
Oceanic crust	0.1×10^{-6}	0.1×10^{-6}	[16]
Upper mantle	$(5 ; 8) \times 10^{-9}$	6.5×10^{-9}	Average of [19], [23]
Lower mantle		13.2×10^{-9}	From Eq. (3) with $a_{\text{BSE}}(\text{U}) = 2 \times 10^{-8}$
Core		0	

TABLE III: Thorium abundances in Earth's interior.

Layer	Available data	Average	Adopted value	Remarks
	Th/U	$\langle \text{Th/U} \rangle$	$a^{\text{ref}}(\text{Th})$	
Oceans & Seawater	0	0	0	[31]
Sediments	4.11	4.11	6.9×10^{-6}	[32]
Upper CC	3.8 ; 3.8 ; 3.9 ; 4.1	3.9	9.8×10^{-6}	Average of [34], [33], [33], [17]
Middle CC	3.8	3.8	6.1×10^{-6}	[34]
Lower CC	3.8 ; 6.0 ; 7.0 ; 7.1	6	3.7×10^{-6}	Average of [16], [34], [25], [17]
Oceanic crust	2.2	2.2	0.22×10^{-6}	[16]
Upper mantle	2.58 ; 2.63 ; 2.7 ; 2.73	2.66	17.3×10^{-9}	Average of [20], [21], [22], [23]
Lower mantle			52.0×10^{-9}	From Eq. (3) with $a_{\text{BSE}}(\text{Th}) = 7.8 \times 10^{-8}$
Core			0	

TABLE IV: Potassium abundances in Earth's interior.

Layer	Available data	Average	Adopted value	Remarks
	$(\text{K/U}) \times 10^{-4}$	$\langle \text{K/U} \rangle \times 10^{-4}$	$a^{\text{ref}}(\text{K})$	
Oceans & Seawater	12.5	12.5	4.0×10^{-4}	[31]
Sediments	1.0	1.0	1.7×10^{-2}	[32]
Upper CC	0.99 ; 1.0 ; 1.03 ; 1.10	1.03	2.57×10^{-2}	Average of [16], [17], [33], [33]
Middle CC	1.04	1.04	1.67×10^{-2}	[34]
Lower CC	1 ; 1.2 ; 1.4	1.2	0.72×10^{-2}	Average of [16], [25], [17]
Oceanic crust	1.25	1.25	0.125×10^{-2}	[16]
Upper mantle			0.78×10^{-4}	From K/U approx. constancy
Lower mantle			1.6×10^{-4}	From Eq. (3) with $a_{\text{BSE}}(\text{K}) = 2.32 \times 10^{-4}$
Core			0	

TABLE V: Uranium: masses, radiogenic heat, and predicted fluxes. Units are 10^{17} kg, TW and 10^6 cm^{-2} s^{-1} , respectively. The reference values, lower and upper limits are labeled as ref, low, and high, respectively. Crust summarizes CC and OC; UM (LM) denotes upper (lower) mantle.

			Himalaya 33° N 85° E	Gran Sasso 42° N 14° E	Kamioka 36° N 137° E	Hawaii 20° N 156° W
	$M(\text{U})$	$H(\text{U})$	Φ_{U}			
Crust low	0.206	1.960	3.337	1.913	1.594	0.218
Crust ref	0.353	3.354	5.710	3.273	2.727	0.373
Crust high	0.413	3.920	6.674	3.826	3.187	0.436
UM low	0.048	0.455	0.146	0.146	0.146	0.146
UM ref	0.062	0.591	0.189	0.189	0.189	0.189
UM high	0.077	0.727	0.233	0.233	0.233	0.233
LM low	0.147	1.399	0.288	0.288	0.288	0.288
LM ref	0.389	3.695	0.760	0.760	0.760	0.760
LM high	1.177	11.182	2.299	2.299	2.299	2.299
Total low	0.401	3.814	3.770	2.346	2.027	0.651
Total ref	0.804	7.639	6.659	4.222	3.676	1.322
Total high	1.666	15.828	9.206	6.358	5.720	2.968

TABLE VI: Thorium: masses, radiogenic heat, and predicted fluxes. Units are 10^{17} kg, TW and 10^6 cm $^{-2}$ s $^{-1}$, respectively. The reference values, lower and upper limits are labeled as ref, low, and high, respectively. Crust summarizes CC and OC; UM (LM) denotes upper (lower) mantle.

			Himalaya 33° N 85° E	Gran Sasso 42° N 14° E	Kamioka 36° N 137° E	Hawaii 20° N 156° W
	$M(\text{Th})$	$H(\text{Th})$	Φ_{Th}			
Crust low	0.838	2.263	2.972	1.714	1.420	0.180
Crust ref	1.450	3.915	5.141	2.964	2.456	0.311
Crust high	1.722	4.649	6.105	3.520	2.916	0.370
UM low	0.124	0.336	0.083	0.083	0.083	0.083
UM ref	0.166	0.447	0.111	0.111	0.111	0.111
UM high	0.207	0.558	0.138	0.138	0.138	0.138
LM low	0.383	1.034	0.165	0.165	0.165	0.165
LM ref	1.532	4.135	0.658	0.658	0.658	0.65
LM high	4.590	12.393	1.973	1.973	1.973	1.973
Total low	1.346	3.633	3.220	1.961	1.668	0.428
Total ref	3.147	8.497	5.910	3.733	3.225	1.080
Total high	6.519	17.600	8.216	5.631	5.028	2.481

TABLE VII: Potassium: masses, radiogenic heat, and predicted fluxes. Units are 10^{21} kg, TW, and $10^6 \text{ cm}^{-2} \text{ s}^{-1}$, respectively. The reference values, lower and upper limits are labelled as ref, low, and high, respectively. Crust summarizes CC and OC; UM (LM) denotes upper (lower) mantle.

			Himalaya 33° N 85° E	Gran Sasso 42° N 14° E	Kamioka 36° N 137° E	Hawaii 20° N 156° W
	$M(\text{K})$	$H(\text{K})$	Φ_{K}			
Crust low	0.210	0.757	12.429	7.126	5.941	0.851
Crust ref	0.367	1.321	21.684	12.432	10.366	1.485
Crust high	0.441	1.587	26.048	14.934	12.451	1.784
UM low	0.057	0.207	0.634	0.634	0.634	0.634
UM ref	0.075	0.269	0.824	0.824	0.824	0.824
UM high	0.092	0.331	1.015	1.015	1.015	1.015
LM low	0.177	0.636	1.254	1.254	1.254	1.25
LM ref	0.471	1.697	3.343	3.343	3.343	3.34
LM high	1.344	4.838	9.534	9.534	9.534	9.534
Total low	0.444	1.600	14.317	9.014	7.829	2.739
Total ref	0.913	3.287	25.852	16.600	14.533	5.652
Total high	1.877	6.756	36.596	25.482	23.000	12.332

TABLE VIII: Differential produced fluxes: the contributions from the crust at Kamioka. The distance R is in km, f_X in $\text{cm}^{-3} \text{s}^{-1}$.

R	f_U	f_{Th}	f_K
10	1.86E-01	1.61E-01	6.94E-01
20	2.29E-01	1.97E-01	8.55E-01
30	2.01E-01	1.75E-01	7.57E-01
40	1.59E-01	1.45E-01	6.07E-01
50	1.23E-01	1.12E-01	4.68E-01
60	9.86E-02	9.04E-02	3.76E-01
70	8.34E-02	7.65E-02	3.18E-01
80	7.51E-02	6.87E-02	2.86E-01
90	6.62E-02	6.06E-02	2.52E-01
100	5.57E-02	5.11E-02	2.12E-01
200	2.31E-02	2.12E-02	8.82E-02
300	8.15E-03	7.39E-03	3.12E-02
400	5.24E-03	4.74E-03	2.01E-02
500	3.68E-03	3.31E-03	1.41E-02
600	2.61E-03	2.35E-03	1.00E-02
700	2.47E-03	2.23E-03	9.50E-03
800	2.53E-03	2.29E-03	9.68E-03
900	2.94E-03	2.67E-03	1.13E-02
1000	2.88E-03	2.61E-03	1.10E-02
2000	1.32E-03	1.20E-03	5.06E-03
3000	1.08E-03	9.72E-04	4.11E-03
4000	1.05E-03	9.51E-04	4.01E-03
5000	7.44E-04	6.75E-04	2.84E-03
6000	4.88E-04	4.40E-04	1.86E-03
7000	4.28E-04	3.86E-04	1.64E-03
8000	2.99E-04	2.69E-04	1.14E-03
9000	2.53E-04	2.27E-04	9.67E-04
10000	2.19E-04	1.98E-04	8.41E-04
11000	2.16E-04	1.96E-04	8.28E-04
12000	1.40E-04	1.24E-04	5.35E-04

TABLE IX: Differential produced fluxes: the contributions from the crust at Gran Sasso. The distance R is in km, f_X in $\text{cm}^{-3} \text{s}^{-1}$.

R	f_U	f_{Th}	f_K
10	1.48E-01	1.29E-01	5.48E-01
20	2.11E-01	1.82E-01	7.86E-01
30	1.80E-01	1.59E-01	6.79E-01
40	1.40E-01	1.28E-01	5.34E-01
50	1.12E-01	1.03E-01	4.26E-01
60	8.94E-02	8.21E-02	3.41E-01
70	7.66E-02	7.04E-02	2.92E-01
80	6.59E-02	6.05E-02	2.51E-01
90	5.92E-02	5.43E-02	2.25E-01
100	5.22E-02	4.79E-02	1.99E-01
200	2.30E-02	2.11E-02	8.75E-02
300	1.31E-02	1.20E-02	5.02E-02
400	1.14E-02	1.04E-02	4.34E-02
500	9.83E-03	8.95E-03	3.74E-02
600	7.52E-03	6.81E-03	2.86E-02
700	5.98E-03	5.43E-03	2.27E-02
800	5.01E-03	4.56E-03	1.91E-02
900	4.95E-03	4.52E-03	1.88E-02
1000	5.12E-03	4.68E-03	1.95E-02
2000	2.98E-03	2.71E-03	1.13E-02
3000	1.60E-03	1.45E-03	6.08E-03
4000	1.22E-03	1.11E-03	4.66E-03
5000	7.65E-04	6.91E-04	2.91E-03
6000	5.98E-04	5.42E-04	2.28E-03
7000	5.66E-04	5.14E-04	2.16E-03
8000	4.44E-04	4.02E-04	1.69E-03
9000	2.20E-04	1.97E-04	8.41E-04
10000	8.20E-05	7.18E-05	3.19E-04
11000	1.61E-04	1.46E-04	6.20E-04
12000	1.27E-04	1.14E-04	4.88E-04

TABLE X: Differential produced fluxes: the contributions from the mantle. The distance R is in km, f_X in $\text{cm}^{-3} \text{s}^{-1}$.

R	f_U	f_{Th}	f_K
10	0.00E+00	0.00E+00	0.00E+00
20	0.00E+00	0.00E+00	0.00E+00
30	0.00E+00	0.00E+00	0.00E+00
40	0.00E+00	0.00E+00	0.00E+00
50	1.62E-04	9.48E-05	7.05E-04
60	2.91E-04	1.70E-04	1.27E-03
70	3.77E-04	2.21E-04	1.64E-03
80	4.38E-04	2.57E-04	1.91E-03
90	4.84E-04	2.83E-04	2.11E-03
100	5.19E-04	3.04E-04	2.26E-03
200	6.64E-04	3.89E-04	2.89E-03
300	7.08E-04	4.14E-04	3.08E-03
400	7.31E-04	4.28E-04	3.19E-03
500	7.53E-04	4.41E-04	3.28E-03
600	7.71E-04	4.51E-04	3.36E-03
700	8.49E-04	5.32E-04	3.70E-03
800	9.83E-04	6.74E-04	4.30E-03
900	1.09E-03	7.83E-04	4.75E-03
1000	1.17E-03	8.70E-04	5.12E-03
2000	1.49E-03	1.22E-03	6.56E-03
3000	1.48E-03	1.24E-03	6.51E-03
4000	1.11E-03	9.27E-04	4.88E-03
5000	8.88E-04	7.41E-04	3.90E-03
6000	7.40E-04	6.17E-04	3.25E-03
7000	6.34E-04	5.29E-04	2.79E-03
8000	5.54E-04	4.63E-04	2.44E-03
9000	4.93E-04	4.11E-04	2.17E-03
10000	4.24E-04	3.53E-04	1.86E-03
11000	2.35E-04	1.91E-04	1.03E-03
12000	6.10E-05	4.11E-05	2.66E-04

TABLE XI: Fractional uncertainties of the produced fluxes.

$\Delta\Phi/\Phi$ (%)	Himalaya	Gran Sasso	Kamioka	Hawaii
conventional 1σ	14	16	17	29

TABLE XII: Total yields. N_{no} is the total number of geoevents (U + Th) in the absence of oscillations predicted from the reference model for 10^{32} proton yr (or in TNU) and ΔN_{no} is the “ 1σ ” error. N_{no}^{low} (N_{no}^{high}) is the minimal (maximal) prediction. For $\delta m^2 > 4 \times 10^{-5}$ eV² the geoevent yield is $N = N_{no} [1 - 0.5 \sin^2(2\theta)]$.

Location	N_{no}	ΔN_{no}	N_{no}^{low}	N_{no}^{high}
Baksan	91	13	51	131
Hawaii	22	6	10	49
Himalaya	112	15	63	154
Homestake	91	13	51	130
Kamioka	61	10	33	96
La Palma	37	8	19	67
LGS	71	11	39	106
Pyhasalmi	92	13	51	131
Sudbury	87	13	48	125
Yucca Mountain	70	11	38	106

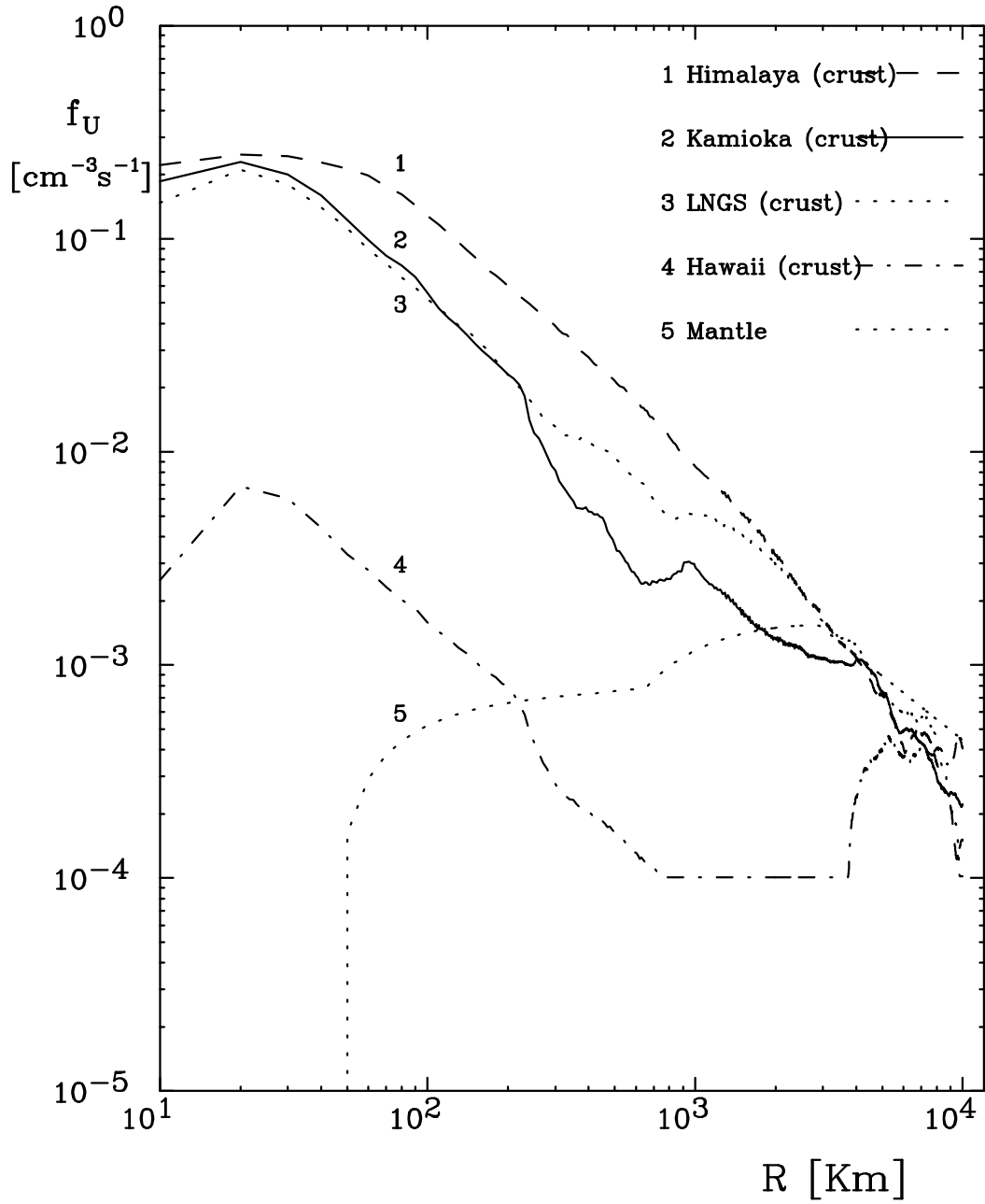


FIG. 1: Differential produced flux from uranium as a function of the distance R from the detector.

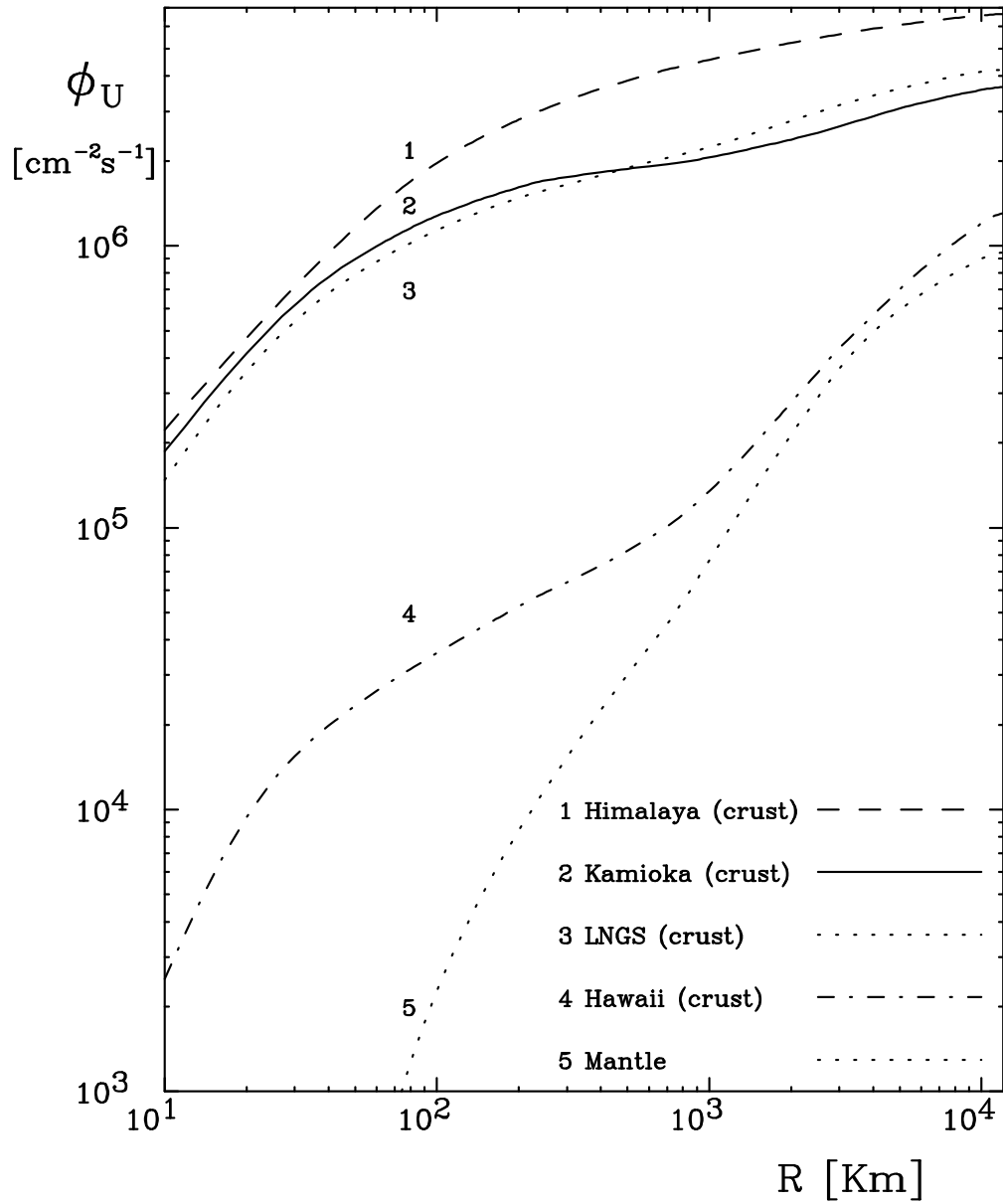


FIG. 2: Cumulated produced flux from uranium as a function of the distance R from the detector.

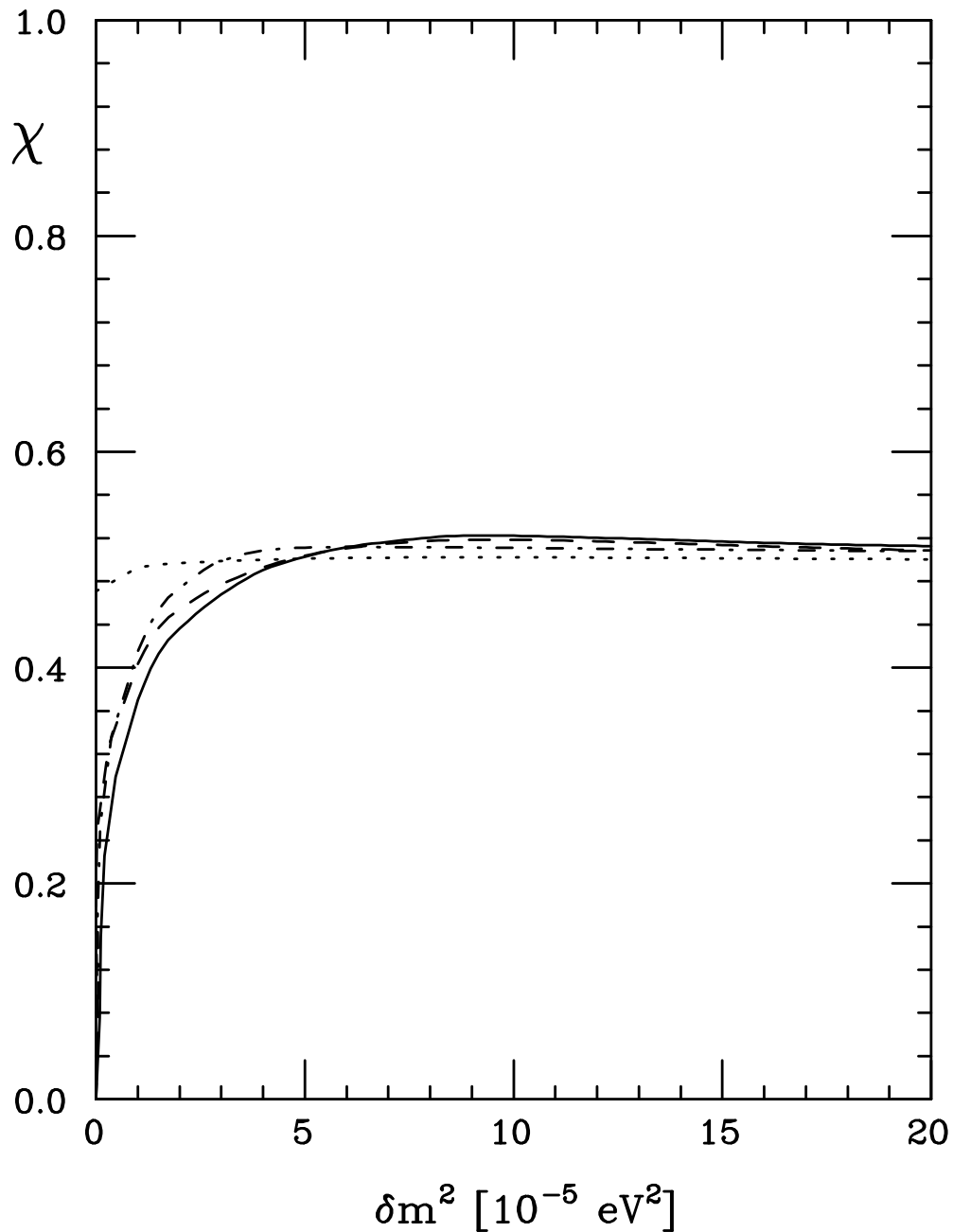


FIG. 3: Dependence of the yield on δm^2 . The figure shows the function $\chi = (N_{\text{no}} - N) / [(N_{\text{no}} \sin^2(2\theta))]$, see Eq. (11), for four locations with δm^2 in units of 10^{-5} eV^2 . Solid (dashed, dotted, dot-dashed) line applies to Kamioka (LNGS, Hawaii, Himalaya).

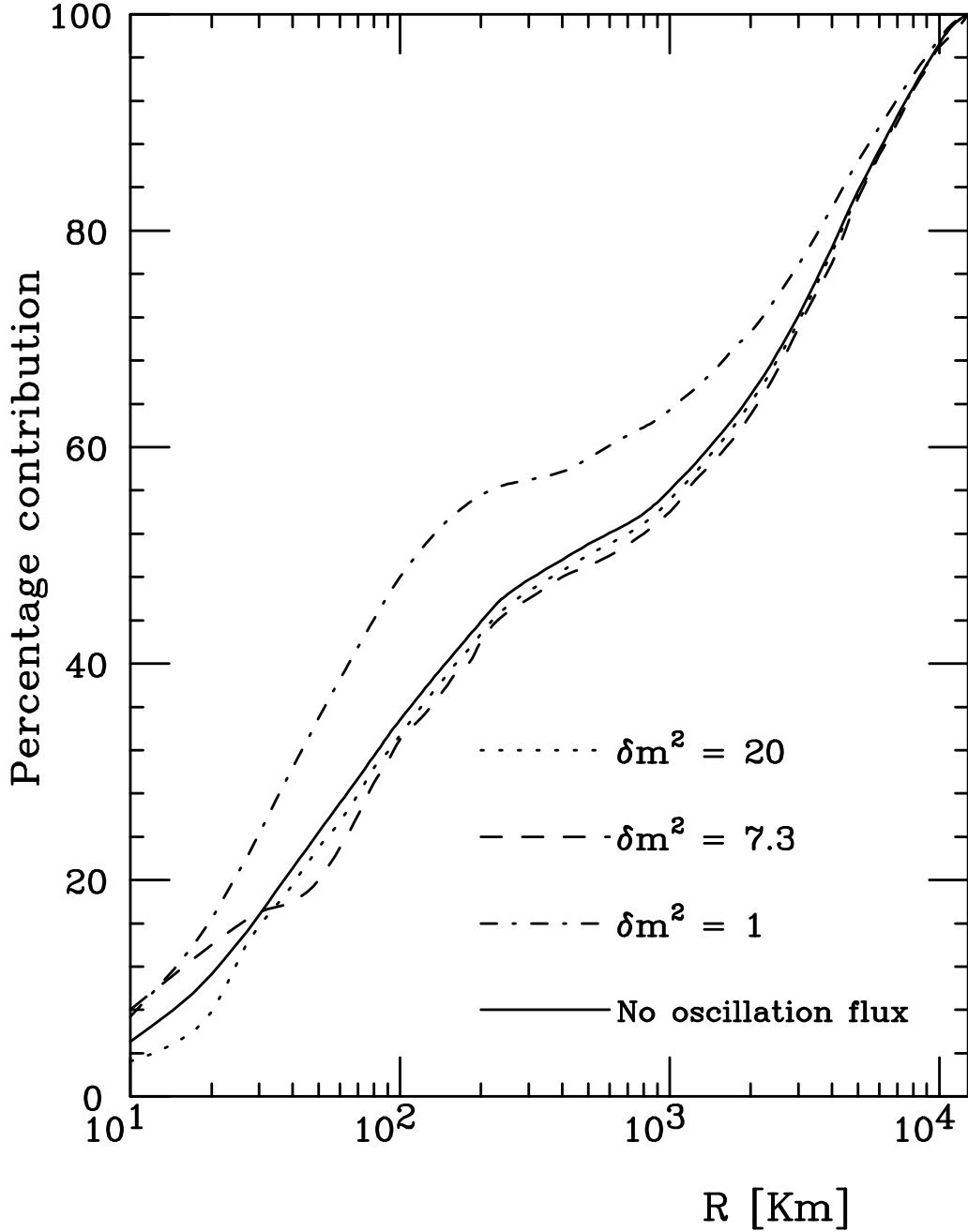


FIG. 4: Contributed signal as a function of distance. The percentage contribution to the event yield at Kamioka originating from sources within R is shown for the indicated values of δm^2 in units of 10^{-5} eV^2 at fixed $\sin^2(2\theta) = 0.863$. The percentage contributed neutrino flux without oscillation is also shown for comparison.

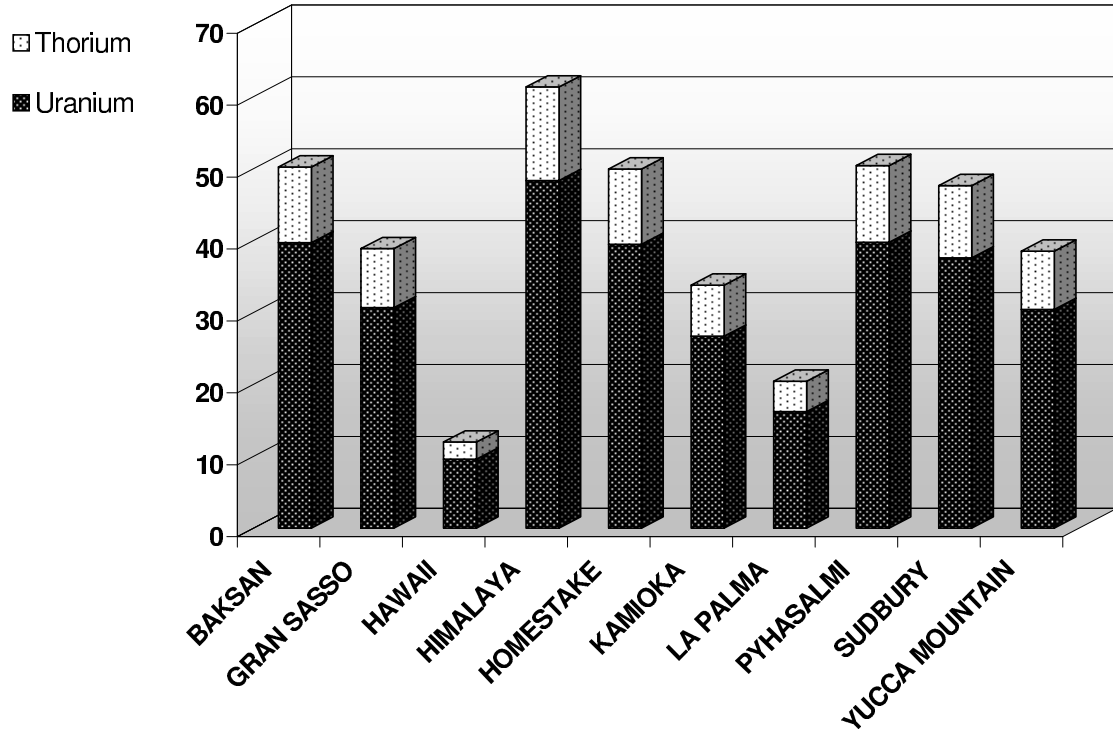


FIG. 5: Yields predicted in the reference model for 10^{32} proton yr, 100% efficiency, assuming the best fit oscillation parameters, $\delta m^2 = 7.3 \times 10^{-5} \text{ eV}^2$ and $\sin^2(2\theta) = 0.863$.

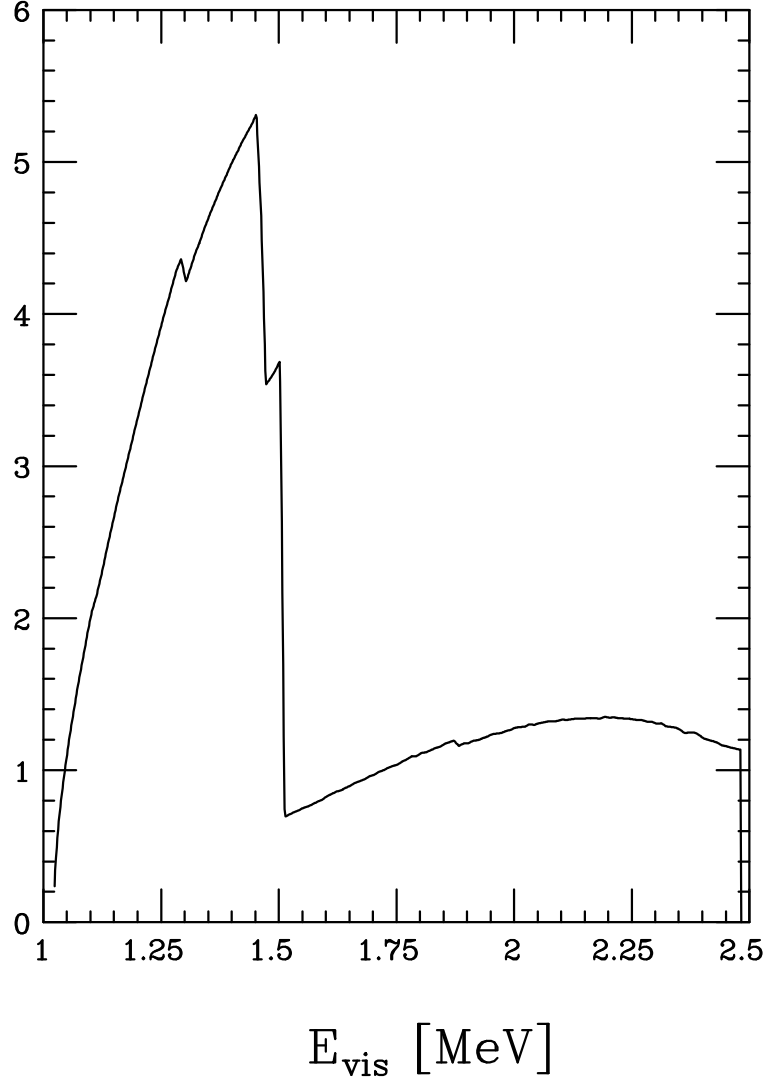


FIG. 6: Event spectrum as function of the visible energy $E_{\text{vis}} = T + 2m_e$ in MeV. The spectrum is calculated for the U/Th flux ratio expected at Kamioka with no oscillation and the normalization is arbitrary.

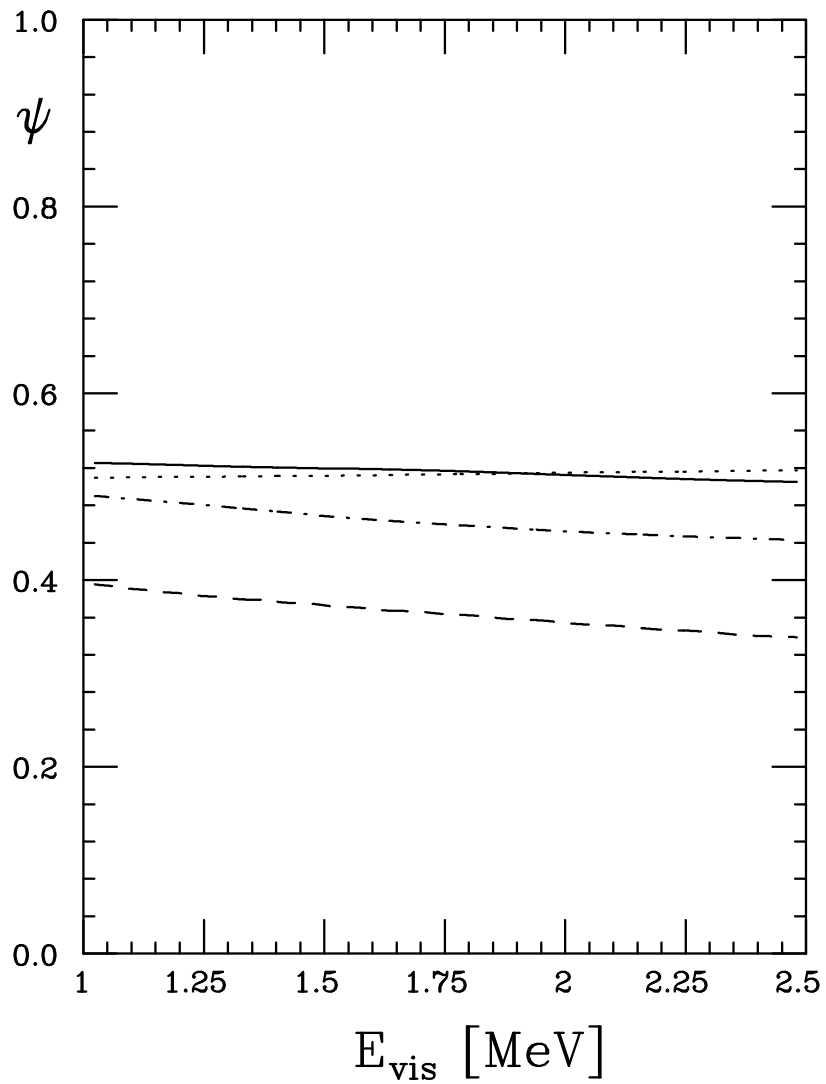


FIG. 7: Spectrum deformation. The function ψ , defined in Eq. (14), as function of the visible energy $E_{\text{vis}} = T + 2m_e$ in MeV for four values of δm^2 : $1 \times 10^{-5} \text{ eV}^2$ (dash line), $3 \times 10^{-5} \text{ eV}^2$ (dot-dash line), $7.3 \times 10^{-5} \text{ eV}^2$ (solid line), and $20 \times 10^{-5} \text{ eV}^2$ (dot line).